ACS APPLIED MATERIALS & INTERFACES

Research Article

www.acsami.org

Tannic Acid Coated Gold Nanorods Demonstrate a Distinctive Form of Endosomal Uptake and Unique Distribution within Cells

Emily A. Untener,[†,‡] Kristen K. Comfort,[†,‡] Elizabeth I. Maurer,[†] Christin M. Grabinski,[†] Donald A. Comfort,[‡] and Saber M. Hussain*[,†]

[†]Molecular Bioffects Branch, Human Effectiveness Directorate, Air Force Research Laboratory, Wright-Patterson Air Force Base, Ohio 45433, United States

[‡]Department of Chemical and Materials Engineering, University of Dayton, Dayton, Ohio 45469, United States

ABSTRACT: One of the primary challenges associated with nanoparticle-dependent biological applications is that endosomal entrapment in a physiological environment severely limits the desired targeting and functionality of the nanoconstructs. This study sought to overcome that challenge through a systematic approach of gold nanorod (GNR) functionalization: evaluating the influence of both aspect ratio and surface chemistry on targeted cellular internalization rates and preservation of particle integrity. Owing to their unique spectral properties and enhanced surface area, GNRs possess great potential for the advancement of nanobased delivery and imaging applications. However, their ability for efficient intracellular delivery while maintaining their specific physiochemical parameters has yet to be satisfactorily explored. This study identified that longer and positively charged GNRs demonstrated a higher degree of internalization compared to their shorter and negative counterparts. Notably, of the four surface chemistries explored, only tannic acid resulted in retention of GNR integrity following endocytosis into keratinocyte cells, due to the presence of a strong protein corona matrix that served to protect the particles. Taken together, these results identify tannic acid functionalized GNRs as a potential candidate for future development in nanobased biomolecule delivery, bioimaging, and therapeutic applications.

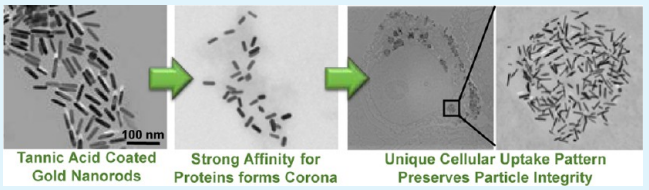

KEYWORDS: *gold nanorod, tannic acid, cellular uptake, endocytosis, protein corona, membrane interaction*

INTRODUCTION

Recently, engineered nanomaterials (NMs) have attracted significant attention due to their innate potential to progress the development of new technologies and increase effectiveness of current biological-based applications, including drug delivery,[1−3] bioimaging techniques,[4−6] and the development of therapeutic agents.[7−10] Due to its perceived inertness, reproducible synthesis procedures, and ease of functionalization, nanogold has demonstrated itself to be an optimal material for these applications.[11,12] In particular, gold nanorods (GNRs) possess a number of shape-specific advantages over nanospheres and other morphologies, including an enhanced surface area and tunable optical properties.[13,14] It is well established that the spectral signature of GNRs extends into the near-infrared (NIR) region, making them an ideal candidate for nanobased applications as biological tissue possesses minimal absorbance in the NIR range.[15,16] Through targeted modification of the GNR size, their dependent optical properties can be precisely tuned, thus creating a mechanism that allows for design of a particle with specific optical properties for a specific function.[17] Additionally, owing to the distinctive composition, shape, and size of GNRs, they display an augmented plasmonic effect, producing a high degree of light scattering that adds to their attractiveness for bioimaging and sensor development techniques.[18]

However, one major obstacle associated with the utilization of GNRs is that the majority of nanobased applications require subcellular delivery to a biological target with high efficiency and specificity.[19] NMs are typically internalized through an endolysosomal mechanism and remain in vesicles that are either marked for degradation or exocytosed from the cell.[20−22] Further complicating this issue is the fact that, once in endosomes or lysosomes, the particles become partially or fully degraded due to the low pH of the lysosomal fluid and the intracellular processes designed for destruction of foreign materials. This loss of particle integrity produces an alteration of the GNR spectral profile and its distinctive characteristics, thus introducing a significant reduction in application effectiveness. As such, finding a mechanism to avoid or account for this spectral shift is a major challenge that must be overcome to progress the development of GNR-based biological applications.[23]

To date, a few studies on nonendosomal delivery of gold nanospheres have been performed,[24] but none have evaluated delivery and integrity of more complex nanoparticles, such as GNRs. Several physical methods have been developed to actively delivery NMs to targeted cellular locations, thus

Received: April 15, 2013
Accepted: August 19, 2013
Published: August 19, 2013

avoiding endosomes and lysosomes, including sonoporation, Genegun, and microinjection techniques.[25−27] However, these methods are invasive, technically challenging, and extremely costly; thus limiting their applicability. As surface chemistry has been strongly correlated to the resultant NM-dependent bioresponses and fate,[28] modification of particle coating has great potential to achieve targeted delivery and maintain stability without the negative traits associated with the aforementioned processes. Moreover, previous studies have investigated the ability of functional groups and surface chemistries to promote NM endosomal release, including viruses, peptides, lipids, and pH sensitive polymers,[29−31] demonstrating the effectiveness of a surface functionalization approach. In addition to surface moieties, NM particle size plays a major role in influencing the mechanism of endocytosis, extent of internalization, and final intracellular fate.[32] Generally speaking, smaller particles are able to more efficiently enter a cell and display cytosolic location.[33,34] Therefore, by exploring combinations of surface chemistry and primary particle size, it may be possible to design a GNR population for the optimization of intracellular particle delivery while simultaneously maintaining spectral integrity.

As such, the goal of this study was to investigate the impact of surface chemistry and aspect ratio (AR) on the degree of GNR internalization and stability within the human keratinocyte, HaCaT, cell line. HaCaT cells were specifically chosen for this investigation, as skin is a first line of defense against NM exposure and a common target organ for nanobased applications. Furthermore, the HaCaT model has been extensively utilized in previous studies exploring NM-dependent responses and has become a model cell line for investigations into intracellular NM fate and behavior.[35−37] In this investigation, GNRs with ARs of 3 and 6 were synthesized, fully characterized, and functionalized with one of four surface chemistries. The functional groups selected for this study were each designed to promote a specific cellular response and included: tannic acid (TA) for stability, TAT peptide (transactivator of transcription) for augmented internalization, TAT HA2 peptide (transactivator of transcription and hemaglutanin) for endosomal release, and carboxylated polyethylene glycol (COOH) for both stability and to eliminate the variable of surface charge. The extent of GNR internalization, final location, spatial orientation, and particle integrity were assessed for each GNR set within HaCaT cells. The results presented here identified that degree of GNR uptake and distribution were mutually dependent on the nanorod size as well as the surface chemistry, as both induced dramatic alterations to the way HaCaT cells perceived the particles. Furthermore, to elucidate the mechanism of HaCaT internalization as a function of surface chemistry, inhibitors were used to block specific routes of endocytosis. Lastly, it was discovered that TA surface chemistry provided a protective coating around the GNRs that resulted in a distinctive form of endocytosis and preserved particle integrity, identifying the tremendous potential of TA functionalization to progress nanobased biological applications.

EXPERIMENTAL SECTION

Cell Culture. The human keratinocyte, HaCaT, cell line was a kind gift from the Army Research Laboratory and was maintained in RPMI 1640 cell culture media (ATCC) supplemented with 10% heat inactivated fetal bovine serum and 1% penicillin-streptomycin. Cells were grown in a humidified incubator controlled at 37 °C and 5% CO_2. The same media composition was used for all GNR exposure procedures.

GNR Synthesis. GNRs of AR 3 were synthesized according to a modified seed mediated procedure reported by Park and Vaia.[38] Briefly, it comprised the combination of two solutions at room temperature: a seed solution and a growth solution, both of which contained 0.1 M cetyltrimethylammonium bromide (CTAB). The seed solution also contained 0.1 M chlorauric acid, while the growth solution included 0.1 M chlorauric acid, 0.1 M silver nitrate, and 0.1 M ascorbic acid. The GNRs of AR 6 were synthesized through the same seed mediated mechanism with the only exception that the growth solution contained 0.1 M benzyldimethylhexadecylammonium chloride (BDAC). Purification of GNRs was achieved using a depletion induced separation procedure utilizing excess BDAC, as previously described.[39] The CTAB was purchased from GFS chemicals. The chloroauric acid, ascorbic acid, silver nitrate, sodium borohydride, and tannic acid were obtained from Sigma Aldrich. The BDAC was purchased from TSI Incorporated.

Functionalization Procedure. GNRs were functionalized through a stepwise addition procedure. First, the particles were functionalized overnight with PEG (0.001 M; Nanocs) to displace the surface bound CTAB molecules. The next day, the samples were centrifuged at 8000*g* and the GNRs were resuspended in a 0.001 M solution of the desired functionalization material; TAT, TAT HA2 (Invitrogen), PEG-COOH (Nanocs), or TA (Sigma Aldrich). After 24 h, the GNR samples were again centrifuged and the supernatant was removed and replaced with sterile water. The specific sequences for TAT and TAT HA2, respectively, are GRKKRRQRRRPQ and RRRQRRKKRGGDIMGEWGNEIFGAIAGFLG. This addition process was repeated twice to ensure full functionalization.

GNR Characterization. UV−vis analysis was performed on a Varian Cary Bio 3000 instrument to determine the purity, stability, and spectral signature of GNRs following synthesis. The rod shape was verified, and the sizes of the GNRs were determined using transmission electron microscopy (TEM) and ImageJ software. The average particle volume was calculated using these obtained length and width measurements ($n > 50$). To assess the surface charge of the GNRs, zeta potential measurements were taken using laser Doppler electrophoresis on a Malvern Zetasizer, Nano-ZS. Agglomerate sizes of the GNRs in media were determined through dynamic light scattering (DLS), also on a Malvern Zetasizer.

Cellular Internalization Studies. HaCaT cells were seeded in a 6-well plate at 1×10^6 cells/well for 24 h then exposed to the stated GNRs (15 μg/mL) for the indicated duration, washed, and fixed overnight in 2% paraformaldehyde and 1% glutaraldehyde. The cells were then stained with 1% osmium tetroxide, washed, and subsequently dehydrated with ethanol dilutions ranging from 50 to 100%. The cells were then encased in LR White resin and cured overnight at 60 °C under a vacuum, after which the samples were sectioned using a Leica EM UC7 Ultramicrotome and imaged via TEM.

Quantification of Intracellular GNRs. A total of 1×10^6 HaCaT cells were seeded in a 6-well plate then dosed with 15 μg/mL GNRs for 24 h. The cell samples were then washed, detached with trypsin, counted, and digested with an aqueous solution containing 0.05% Triton X-100, 3% HCl, and 1% HNO_3. The intracellular gold concentration was determined through inductively coupled plasma mass spectrometry (ICP-MS) on a Perkin-Elmer ICP-MS 300D instrument.

For endocytosis inhibitor studies, HaCaT cells were exposed to an appropriate concentration of inhibitors for 1 h prior to the introduction of 15 μg/mL GNRs for 3 h. The inhibitors and concentration used were 400 μmol/L genistein (Sigma Aldrich), 200 μmol/L 5-(*N*-ethyl-*N*-isopropyl)amiloride (EIPA; Sigma Aldrich), 31 μmol/L chlorpromazine (Sigma Aldrich), and incubation at 4 °C. Cells were then washed and the aforementioned procedure for ICP-MS was used to quantify cellular uptake.

Cellular Viability Assessment. HaCaT cell viability was evaluated using the CellTiter 96 Aqueous One Solution (Promega) which monitors mitochondrial function. Cells were seeded into a 96-well

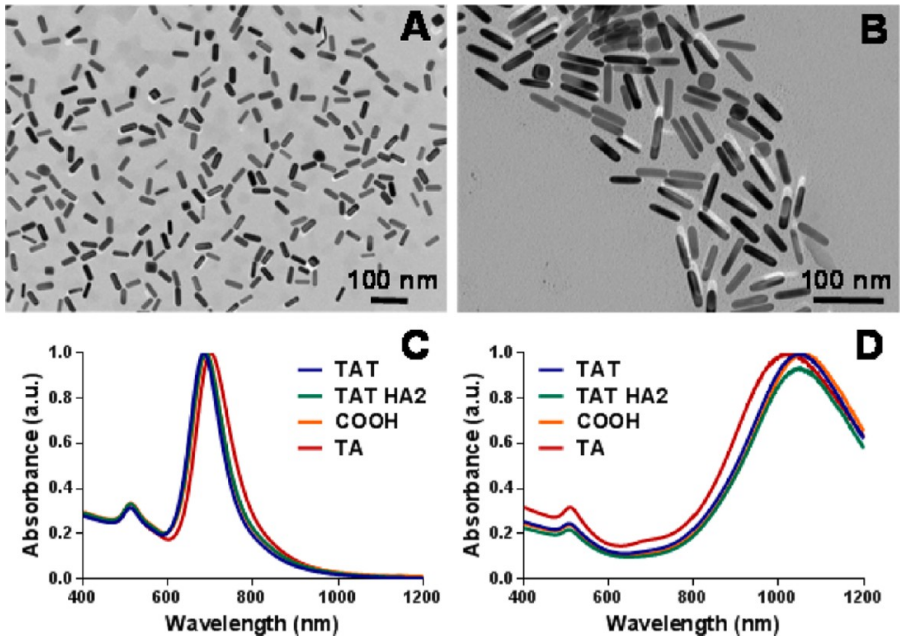

Figure 1. Characterization of gold nanorods. Representative TEM images of GNRs following synthesis and purification of (A) AR 3 and (B) AR 6 demonstrated excellent particle uniformity and a rod-shaped morphology. UV−vis analysis was performed in water to verify that surface functionalization induced negligible alterations to the GNR spectral properties for both (C) AR 3 and (D) AR 6.

plate at a concentration of 2×10^4 cells per well and the following day treated with the stated GNR conditions. After 24 h, the cells were washed and viability was determined in accordance with the manufacturer's protocol.

CytoViva Imaging. HaCaT cells were seeded at 2×10^5 cells per chamber on a 2-well chambered slide and grown for 24 h. Cells that were undergoing cold incubation were placed at 4 °C for 1 h prior to the introduction of TA GNRs at a concentration of 15 μg/mL. After 3 h, the cells were fixed with 4% paraformaldehyde and incubated with Alexa Fluor 555-phalloidin for actin staining and DAPI for nuclear staining (Invitrogen). The slides were then sealed and imaged using a CytoViva 150 ultraresolution attachment on an Olympus BX41 microscope (Aetos Technologies, Inc.).

Statistical Analysis. Data is expressed as the mean ± the standard error of the mean (SEM). A one-way ANOVA analysis was run using Graph Pad Prism followed by a Bonferroni adjustment to determine statistical significance between GNR sets with an asterisk denoting a p value of <0.05.

RESULTS AND DISCUSSION

Gold Nanorod Characterization. The experimental matrix designed for this study investigated GNRs with ARs 3 and 6, each functionalized with TAT, TAT HA2, COOH or TA. Following synthesis of these GNR sets, full characterization was performed to determine their specific physicochemical properties and verify particle uniformity. First, TEM was used to visualize the particles to confirm rod-shaped morphology and ascertain precise size measurements. As seen in Figure 1A and B, representative TEM images demonstrated that both GNR sets were uniform in size and shape. The variance of GNR optical properties as a function of AR are well-defined with the longitudinal peak shifting to the right with increased AR.[40] Our results are in agreement with previous reports, as the longitudinal peak of AR 6 was located further into the NIR spectrum then that of AR 3. Furthermore, UV−vis analysis confirmed that functionalization did not significantly alter particle size or stability (Figure 1C and D), as minimal alterations were noted. A slight shift was observed with TA functionalization, with nominal shifts associated with TAT, TAT HA2, and COOH. GNR uniformity was further confirmed from TEM imaging, as the particles displayed an even size distribution even after functionalization (Table 1). Furthermore, average particle length and width were calculated from TEM images for each GNR set and used to calculate particle volumes (Table 1).

Table 1. Physical Properties of Gold Nanorods

AR	surface chemistry	avg length (nm)	avg diameter (nm)	avg AR	particle volume (nm^3)	surface charge (mV)
3	TAT	42.5	13.7	3.11 ± 0.52	5989	8.4
3	TAT HA2	43.9	14.4	3.06 ± 0.41	6365	9.2
3	COOH	41.7	13.9	3.00 ± 0.60	5622	−18.5
3	TA	43.4	14.4	3.02 ± 0.47	6283	−19.7
6	TAT	63.5	10.5	6.04 ± 0.47	5193	9.5
6	TAT HA2	63.1	10.2	6.19 ± 0.42	4876	11.8
6	COOH	64.8	10.9	5.94 ± 0.49	5705	−17.6
6	TA	64.1	10.8	5.95 ± 0.47	5540	−25.2

To assess GNR surface charge following functionalization, a zeta potential analysis was performed on each particle set (Table 1). From this analysis, it was shown that TAT and TAT HA2 resulted in positively charged GNRs whereas COOH and TA coated GNRS displayed a negative surface charge. Moreover, the zeta potential results associated with ARs 3 and 6 are in excellent agreement with each other, further demonstrating complete and effective functionalization of all particle sets in this study. For TAT, TAT HA2, and COOH, the thiolated surface chemistry displaces the CTAB from the surface of the GNR. However, TA does not have a strong enough affinity for gold to remove the CTAB, but instead, has been shown to overcoat the particles, effectively blocking the cytotoxic implications of CTAB.[41]

Dependence of GNR Uptake on Size and Surface Chemistry. Next, the extent of GNR cellular uptake, as a function of both AR and surface chemistry, was quantified after a 24 h exposure (Figure 2A). These results identified that

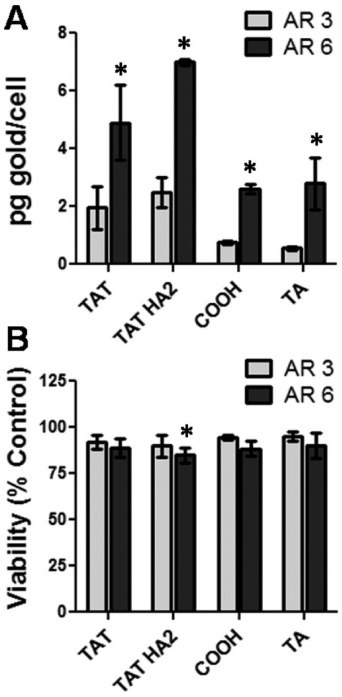

Figure 2. (A) Extent of GNR internalization by HaCaT cells following a 24 h exposure at a concentration of 15 μg/mL. For all employed surface coatings, there was a substantial increase in cellular uptake for AR 6 versus AR 3 (n = 3, asterisk (*) denotes statistically significant difference between aspect ratios, $p < 0.05$). (B) Cellular viability was assessed after a 24 h exposure to 50 μg/mL GNRs dosages. The only GNR set to induce a slight, but statistically significant drop in viability was AR 6 TAT HA2 functionalized. (n = 4, asterisk (*) denotes statistical significance from untreated control, $p < 0.05$).

independent of size, the positively charged TAT and TAT HA2 GNRs were internalized at a higher rate compared to the negatively charged TA or COOH GNRs. This charge-dependent phenomenon has been seen previously and is hypothesized to be due to the fact that the cellular membrane is negatively charged and positively charged species would have a greater attraction, thus resulting in augmented internalization.[42]

In addition to GNR internalization being dependent on surface charge, the results presented in Figure 2A indicated that uptake is also influenced by AR, as AR 6 GNRs demonstrated higher uptake ability over AR 3 for all tested functionalizations. Numerous reports have determined that smaller particles are internalized more efficiently than their larger counterparts, which initially contradicts these results.[42] However, AR is calculated by dividing the particle length by its diameter and is not necessarily a metric of actual size. From Table 1, it can be seen that, on a volume basis, AR 3 is actually larger than AR 6 with average particle volumes of 6065 and 5328 nm^3, respectively. When viewed in the context of volume and not AR, these results parallel previously published internalization trends, and highlight the importance of proper NM characterization to truly elucidated and understand their bioresponses.

In addition to extent of internalization, the biocompatibility of the GNR sets was explored in the HaCaT cell line (Figure 2B). At a high GNR concentration of 50 μg/mL, minimal cytotoxicity existed, with the only exception being a 15% induction of cell death associated with the TAT HA2 functionalized AR 6 GNRs. Interestingly, this loss in viability correlated with the GNR set in which particles were internalized most efficiently (Figure 2A), emphasizing the critical link between cellular-particle association and nanotoxicity.

Unique Intracellular Distribution of TA GNRs. Using TEM imaging analysis, the intracellular location of GNRs was assessed following a 24 h incubation with 15 μg/mL of each particle set. TEM data demonstrated definitive uptake of GNRs for all examined scenarios (Figure 3) with more visible particles seen with AR 6 GNRs, in agreement with the previous ICP-MS results. Starting with AR 3 (Figure 3A–D), TAT, TAT HA2, and COOH GNRS were found to be localized within intracellular vesicles, likely endosomes. With TA GNRs, some particles are clearly localized within vesicles, while others were identified distributed through the cell, rather in dense agglomerates. For AR 6 GNRs (Figure 3E–H), larger, extremely compact agglomerates of TAT, TAT HA2, and COOH particles were found within HaCaT cells. However, as with AR 3, the TA GNRs possessed a unique, dispersed particle intracellular distribution (Figure 3H). This distinct intracellular fate could be due to the high affinity that serum proteins have for TA,[43] potentially creating a protein matrix around the GNRs.

From these images, it can clearly be seen that TAT, TAT HA2, and COOH GNRs become fused together and lose their distinctive particle characteristics following internalization. However, because of the protein corona surrounding TA GNRs, these particles are able to retain individual, dispersed stability following internalization. While this response is not as pronounced with AR 3, some particle fusing is still visible with the TAT and TAT HA2 samples, but not observed with TA. As we hypothesized that these distinctive behavior patterns associated with TA GNRs were due to the presence of and interaction with a protein corona, further studies exploring this supposition were performed.

Using ImageJ software, this distribution phenomenon was further examined by converting Figure 3F1 and H1 to binary images and used to determine the particle area fraction of the GNRs (Figure 4). From this analysis, it was revealed that TA GNRs possessed a particle area fraction of 25.3 whereas TAT HA2 had a fraction of 51.5. These findings numerically support our hypothesis that TA functionalization results in the formation of a protein corona that protects the particles and maintains their individual integrity. However, with the other functionalizations, the GNRs become fused together following entry into the cells, resulting in a loss of distinctive spectral properties and characteristics that make nanorods advantageous for biobased applications.

Correlation of Surface Chemistry to Endocytosis Mechanism. Gold nanoparticles are believed to enter the cell through a combination of different forms of endocytosis, the exact mechanisms of which remain unclear. Therefore, in addition to examining the mass of GNRs uptaken, it is also crucial to understand the mechanism through which nanorods are entering the HaCaT cells. As we wished to explore the role surface chemistry plays in endocytosis and due to the fact that mode of interaction is dominated by surface chemistry, only one AR was evaluated from this point forward. Owing to the increased frequency of use, augmented particle stability, and

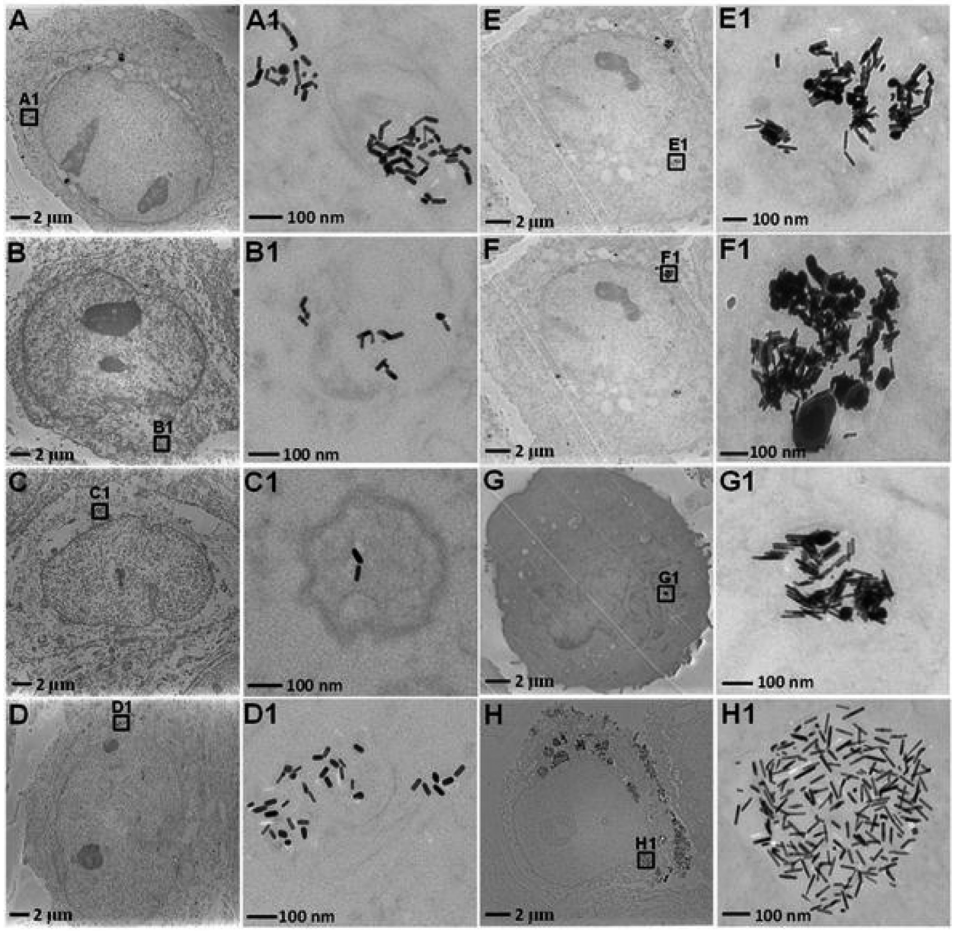

Figure 3. Intracellular fate of gold nanorods is dependent on surface functionalization. Qualitative evaluation of GNR intracellular fate was performed via TEM imaging. Representative images are shown for AR 3 functionalized with (A) TAT, (B) TAT HA2, (C) COOH, and (D) TA. Demonstrative TEM images are included for AR 6 GNRs with the surface chemistries of (E) TAT, (F) TAT HA2, (G) COOH, and (H) TA. The area indicated by the box has been enlarged to more accurately assess the existence of intracellular vacuoles and GNR behavior patterns.

Figure 4. Unique intracellular distribution of tannic acid GNRs. TEM images of (A) TAT HA2 GNRs and (B) TA GNRs were converted to binary images to assess the spatial orientation of aspect ratio 6 GNRs within HaCaT cells. From these results, the particle area fractions were determined in order to evaluate the preservation of GNR particle integrity. With TA functionalization, nanorod morphology is maintained, whereas GNRs were found to fuse together with TAT HA2 surface coating.

higher yield during synthesis, AR 3 GNRs were selected for investigation.

In an effort to elucidate whether and which types of endocytosis were being activated during GNR internalization, inhibitors were employed that blocked specific endocytic pathways: chlorpromazine (Chlor), 5-(*N*-ethyl-*N*-isopropyl)-amiloride (EIPA), genistein (Gen), and incubation at 4 °C. These first three inhibitors block clathrin-mediated endocytosis, macropinocytosis, and caveolae-dependent endocytosis, respectively.[44,45] Cellular incubation at 4 °C disrupts energy dependent uptake, which would include all forms of endocytosis and should produce a severe diminishment in the rate of particle internalization.[46]

Through application of these inhibitors, it was identified that GNRs were internalized through a number of mechanisms, with each surface functionalization relying on a unique combination of processes (Figure 5). TAT and TAT HA2 were uptaken primarily through macropinocytosis and clathrin-mediated endocytosis, and as expected displayed minimal GNR internalization at 4 °C. In literature, macropinocytosis has been shown as the dominant method of entry for positively charged and large nanoparticles,[47] in agreement with our findings. It has also been found that adsorption of serum proteins leads to particle agglomeration and internalization through receptor-mediated endocytosis, of which clathrin-dependent endocytosis is a specific subset.[48] COOH GNRs appeared to be internalized through a combination of multiple endocytosis mechanisms, without a dominant method, as uptake was reduced by all inhibitors examined. Lastly, and most intriguingly, the rate of TA GNR internalization was not significantly impacted by any of the utilized inhibitors, including incubation at 4 °C. While the results associated with TAT, TAT HA2, and COOH GNRs demonstrated their distinctive internalization as a function of specific endocytic pathways, the TA results follow no known pattern of nanoparticle uptake. As these particles are large, that

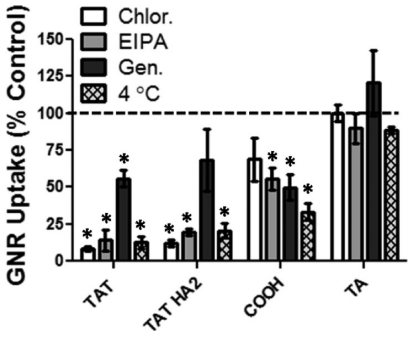

Figure 5. Evaluation of internalization mechanism through the employment of endocytosis inhibitors. Following incubation with endocytosis inhibitors, the internalization rate of AR 3 GNRs was assessed in HaCaT cells through ICP-MS evaluation and compared against GNR exposed cells without inhibitors. (n = 3, asterisk (∗) denotes statistically significant difference from control, p < 0.05).

is to say not on the order of single digit nanometer size, it is highly unlikely that they would enter HaCaT cells through direct diffusion. As such, these results combined with previous TEM images demonstrated the need for further exploration concerning the interactions between tannic acid and HaCaT cells.

Evaluation of Tannic Acid GNR Behavior Patterns. The first step taken in investigating the unique behavior of TA GNRs was to examine the extent of GNR agglomeration in biological medium, as particle aggregation patterns impact how the cells perceive and interact with NMs (Figure 6A–D). From both the shown TEM images and the included DLS size data, TA GNRs displayed an augmented agglomerate size in media over the other three examined functionalizations. As expected, TAT, TAT HA2, and COOH GNRs agglomerated to a small degree, approximately 100 nm, as all NMs will agglomerate to some degree in highly conductive solution.[49] On the contrary, TA coating resulted in the formation of a strong, visible protein corona that encased the GNRs in a matrix with a high effective diameter and low degree of interparticle interactions. The formation of this large corona is due to the well-documented, strong affinity that tannic acid displays for proteins.[43] Thus, GNRs functionalized with tannic acid resulted in the unique combination of a strong protein attraction and the distinctive nanogold physiochemical properties, producing an enhanced corona effect.

Next, UV–vis analysis of the GNRs in media was performed to determine if particle agglomeration induced a spectral shift (Figure 6E). Agglomeration has been shown to induce a number of alterations to the spectral signatures of nanorods, including a red-shift and broadening of the longitudinal surface plasmon peak. While the optical properties of TAT, TAT HA2, and COOH GNRs in media were nearly identical, a significant modification was found with TA GNRs. Specifically, tannic acid induced agglomeration resulted in a shift of the longitudinal peak 25 nm further in the NIR spectrum coupled with a slight peak broadening versus the other examined surface functionalizations. Based off the nearly 4-fold increase in agglomerate size associated with TA GNRs, this spectral alteration was not wholly unexpected.

Due to its high affinity for proteins, tannic acid has been shown to tightly associate with the cellular membrane and is frequently employed in enhancement of membrane staining procedures.[43,50] As such, we hypothesized that during the

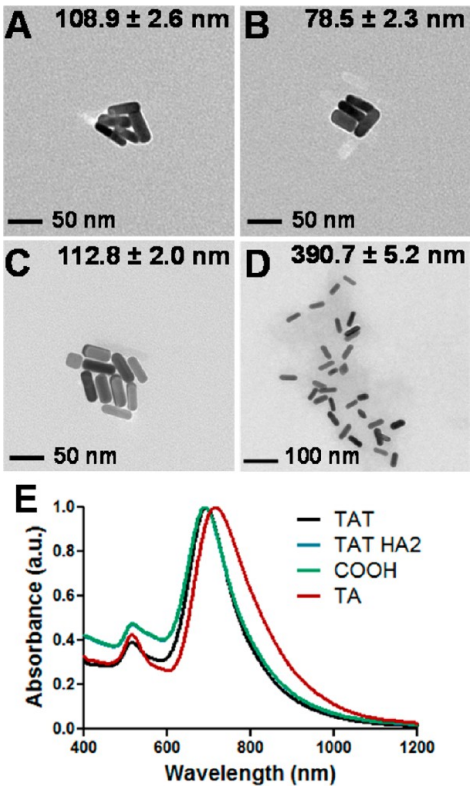

Figure 6. Gold nanorod agglomeration patterns following dispersion in a protein rich environment are dependent on surface coating. The extent of particle aggregation in media was determined both quantitatively and qualitatively through DLS and TEM imaging, respectively. Representative images are shown from GNRs functionalized with (A) TAT, (B) TAT HA2, (C) COOH, and (D) TA. (E) UV–vis spectral signatures of each GNR set in media demonstrated that the TA induced agglomeration resulted in a red-shift of the spectral profile.

endocytosis inhibitor experimentation the TA GNRs were binding tightly to the external membrane of the HaCaT cells, without actually being internalized. Owing to this enhanced protein interactions and distinctive corona associated with TA GNRs, it is highly probable that the washing steps did not successfully remove the external particle agglomerates, resulting in the appearance of no change in intracellular gold.

To test this hypothesis, HaCaT cells were exposed to TA GNRs both at 37 and 4 °C, after which the nanocellular interface was assessed through TEM imaging (Figure 7). Analogous to the previous TA GNR images at 37 °C, the particles were found well inside the outer cell membrane (Figure 7A), indicating full endocytosis activity. Furthermore, distinctive particles are still recognizable as the TA again prevented the fusing of GNRs together. However at 4 °C, TEM images revealed that TA GNRs were in fact associating with the membrane, but not undergoing endocytosis. In addition to identifying the extracellular location of TA GNRs in Figure 7B1, the distinctive protein corona associated with these particles can clearly be visualized, even within a cellular environment. This distribution occurrence was further explored using high resolution fluorescence microscopy, again at both 37 and 4 °C (Figure 7C and D). From these demonstrative images, it appears that the distribution pattern of GNR varies as a function of temperature. At 37 °C the particles are more distributed, however, at 4 °C clustered agglomerates are

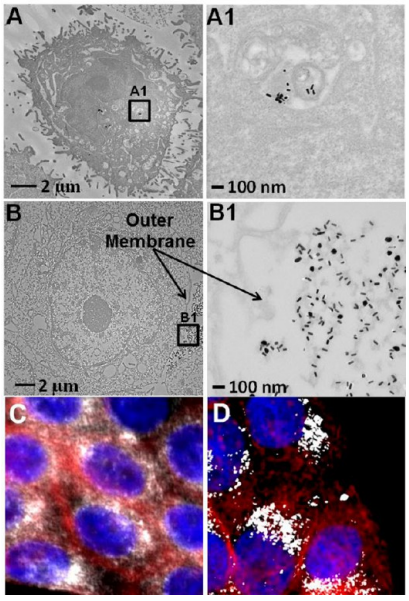

Figure 7. Evaluation of the nanocellular interface with tannic acid functionalized GNRs. Representative TEM images display the cellular location of TA GNRs following incubation at (A) 37 °C and (B) 4 °C. The areas indicated by the box contain the GNRs and are displayed at a higher magnification. Ultrahigh resolution microscopy depicts the interactions between HaCaT cells and TA GNRs at (C) 37 °C and (D) 4 °C. In these images, actin and nuclear stains appear red and blue, respectively, while GNRs are white.

identified. These GNR aggregates appear comparable to the configuration of TA GNRs identified in Figure 7B1. Taken together, we conclude that while TAT, TAT HA2, and COOH GNRs are internalized through standard endocytosis mechanisms, TA GNRs form loosely packed aggregates that appear to fuse with the cellular membrane then undergo a unique endocytosis process.

CONCLUSIONS

GNRs of AR 3 and AR 6 were successfully synthesized, purified, and functionalized with TAT, TAT HA2, COOH, and TA. It was determined that, on a volume basis, the AR 6 particles were smaller than AR 3 particles and displayed an augmented cellular internalization over their shorter counterparts, assessed through intracellular gold concentration. Uptake into HaCaT cells was highly dependent on surface chemistry and charge, with positively charged GNRs (TAT and TAT HA2) having significantly higher uptake than negatively charged particles (COOH and TA). Moreover, mechanisms of endocytosis were explored and found to be dictated by surface chemistry. While TAT, TAT HA2, and COOH GNRs entered HaCaT cells through a combination of normal endocytic pathways, TA coated particles did not appear to be internalized through a traditional mechanism. It was discovered that when functionalized with tannic acid, a protective protein corona formed around the GNRs that resulted in a distinctive form of endocytosis driven by a strong binding between tannic acid and the HaCaT membrane. This corona was also critical in the protection of GNRs and allowed for the retention of particle integrity within a cellular environment. Taken together, the results from this study identified tannic acid as an optimal surface coating for the enhancement of GNR stability and preservation of the distinctive spectral and physiochemical properties needed for nanobased biological applications.

AUTHOR INFORMATION

Corresponding Author

*Tel: 937-904-9517. Fax: 937-904-9610. E-mail: saber.hussain@wpafb.af.mil.

Author Contributions

E.A.U. and K.K.C. contributed equally to this work. The manuscript was written through contributions of all authors. All authors have given approval to the final version of the manuscript.

Notes

The authors declare no competing financial interest.

ACKNOWLEDGMENTS

We would also like to thank Dr. Kyoungweon Park (AFRL/RXAS) for teaching us her GNR synthesis and functionalization techniques. This work was supported in part by the Air Force Surgeon General. E.A.U. was funded in part through the Dayton Area Graduate Studies Institute as well as Oak Ridge Institute for Science and Education (ORISE). E.I.M. and C.M.G. were supported through the Henry Jackson Foundation and ORISE, respectively.

REFERENCES

(1) Wang, Q.; Bao, Y.; Ahire, J.; Chao, Y. *Adv. Healthcare Mater.* **2012**, *2*, 459−466.
(2) Asai, T. *Biol. Pharm. Bull.* **2012**, *11*, 1855−61.
(3) Chen, C.; Lin, Y. P.; Wang, C. W.; Tzeng, H. C.; Wu, C. H.; Chen, Y. C.; Chen, C. P.; Chen, L. C.; Wu, Y. C. *J. Am. Chem. Soc.* **2006**, *128*, 3709−3715.
(4) Cao, C. J.; Li, D. R.; Chen, C. X.; Yang, X. Y.; Hu, J.; Yang, Y.; Zhang, C. Y. *J. Biomed. Opt.* **2012**, *17*, 126002.
(5) Kimura, Y.; Kamisuqi, R.; Narazaki, M.; Matsuda, T.; Tabata, Y.; Toshimitsu, A.; Kondo, T. *Adv. Healthcare Mater.* **2012**, *5*, 657−660.
(6) Liu, T. Y.; Wu, M. Y.; Lin, M. H.; Yang, F. Y. *Acta Biomater.* **2013**, *9*, 5453−5463.
(7) Chen, C. L.; Kuo, L. R.; Lee, S. Y.; Hwu, Y. K.; Chou, S. W.; Chen, C. C.; Chang, F. H.; Lin, K. H.; Tsai, D. H.; Chen, Y. Y. *Biomaterials* **2013**, *34*, 1128−1134.
(8) Xu, Y.; Karmakar, A.; Herberlein, W. E.; Mustafa, T.; Biris, A. R.; Biris, A. S. *Adv. Healthcare Mater.* **2012**, *4*, 493−501.
(9) El-Sayed, I.; Huang, X.; El-Sayed, M. A. *Cancer Lett.* **2006**, *2*, 129−135.
(10) Stern, J.; Stanfield, J.; Kabbani, W.; Hsieh, J. T.; Cadeddu, J. *J. Urol.* **2008**, *179*, 748−753.
(11) Dykman, L.; Khlebtsov, J. N. *Chem. Soc. Rev.* **2012**, *6*, 2256−2282.
(12) Pissuwan, D.; Niidome, T.; Cortie, M. B. *J. Controlled Release* **2011**, *1*, 65−71.
(13) Huang, X.; Neretina, S.; El-Sayed, M. A. *Adv. Mater.* **2009**, *21*, 4880−4910.
(14) DeBrosse, M. C.; Comfort, K. K.; Untener, E. A.; Comfort, D. A.; Hussain, S. M. *Mater. Sci. Eng., C* **2013**, *33*, 4094−4100.
(15) Choi, W. I.; Sahu, A.; Kim, Y. H.; Tae, G. *Ann. Biomed. Eng.* **2012**, *2*, 534−546.
(16) Huang, X.; El-Sayed, I. H.; Qian, W.; El-Sayed, M. A. *J. Am. Chem. Soc.* **2006**, *6*, 2115−2120.
(17) Ng, K. C.; Cheng, W. *Nanotechnology* **2012**, *10*, 105602.
(18) Jain, P. K.; Lee, K. S.; El-Sayed, I. H.; El-Sayed, M. A. *J. Phys. Chem.B* **2006**, *110*, 7238−7248.
(19) Singh, S.; Sharma, A.; Robertson, G. P. *Cancer Res.* **2012**, *22*, 5663−5668.

(20) Kim, J. S.; Yoon, T. J.; Yu, K. N.; Noh, M. S.; Woo, M.; Kim, B. G.; Lee, K. H.; Sohn, B. H.; Park, S. B.; Lee, J. K.; Cho, M. H. *J. Vet. Sci.* **2006**, *4*, 321−326.
(21) Panyam, J.; Labhasetwar, V. *Pharm. Res.* **2003**, *20*, 212−220.
(22) Shukla, R.; Bansal, V.; Chaudhary, M.; Basu, A.; Bhonde, R. R.; Sastry, M. *Langmuir* **2005**, *21*, 10644−10654.
(23) Stacy, B. M.; Comfort, K. K.; Comfort, D. A.; Hussain, S. M. *Plasmonics* **2013**, *8*, 1235−1240.
(24) Taylor, U.; Klein, S.; Petersen, S.; Kues, W.; Barcikowski, S.; Rath, D. *Cytometry, Part A* **2010**, *77*, 439−446.
(25) Li, Y. H.; Shi, Q. S.; Du, J.; Jin, L. F.; Du, L. F.; Liu, P. F.; Duan, Y. R. *Int. J. Mol. Med.* **2013**, *1*, 163−171.
(26) Delehanty, J. B.; Bradburne, C. E.; Susumu, K.; Boeneman, K.; Mei, B. C.; Farrell, D.; Blanco-Canosa, J. B.; Dawson, P. E.; Mattoussi, H.; Medintz, I. L. *J. Am. Chem. Soc.* **2011**, *133*, 10482−10489.
(27) Levy, R.; Shaheen, U.; Cesbron, Y.; See, V. *Nano Rev.* **2010**, *1*, 1−18.
(28) Lundqvisst, M.; Stigler, J.; Elia, G.; Lynch, I.; Cedervall, T.; Dawson, K. A. *Proc. Natl. Acad. Sci. U.S.A.* **2008**, *105*, 14265−14270.
(29) Nativo, P.; Prior, I. A.; Brust, M. *ACS Nano* **2008**, *2*, 1639−1644.
(30) Verma, A.; Uzun, O.; Hu, Y.; Hu, Y.; Han, H. S.; Watson, N.; Chen, S.; Irvine, D. J.; Stellacci, F. *Nat. Mater.* **2008**, *7*, 588−595.
(31) Chou, L.; Ming, K.; Chan, W. *Chem. Soc. Rev.* **2011**, *40*, 233−245.
(32) Aillon, K. L.; Xie, Y.; El-Gendy, N.; Berkland, C. J.; Forrest, M. L. *Adv. Drug Delivery Rev.* **2009**, *61*, 457−466.
(33) Jiang, W.; Kim, B. Y. S.; Rutka, J. T.; Chan, W. C. W. *Nat. Nanotechnol.* **2008**, *3*, 145−150.
(34) Bregar, V. B.; Lojk, J.; Sustar, V.; Veranic, P.; Pavlin, M. *Int. J. Nanomed.* **2013**, *8*, 919−931.
(35) Schaeublin, N. M.; Braydich-Stolle, L. K.; Maurer, E. I.; Park, K.; MacCuspie, R. I.; Afrooz, A. R. M.; Vaia, R. A.; Saleh, N. B.; Hussain, S. M. *Langmuir* **2012**, *28*, 3248−3258.
(36) Comfort, K. K.; Maurer, E. I.; Hussain, S. M. *Bioelectromagnetics* **2013**, DOI: 10.1002/bem.21790.
(37) Yin, J. J.; Liu, J.; Ehrenshaft, M.; Roberts, J. E.; Fu, P. P.; Mason, R. P.; Zhao, B. *Toxicol. Appl. Pharmacol.* **2012**, *263*, 81−88.
(38) Park, K.; Vaia, R. A. *Adv. Mater.* **2008**, *20*, 3882−3886.
(39) Park, K.; Koerner, H.; Vaia, R. *Nano Lett.* **2010**, *10*, 1433−1439.
(40) Link, S.; Mohamed, M. B.; El-Sayed, M. A. *J Phys. Chem. B* **1999**, *103*, 3073−3077.
(41) Alkilany, A. M.; Nagaria, P. K.; Hexel, C. R.; Shaw, T. J.; Murphy, C. J. *Small* **2009**, *5*, 701−708.
(42) Chen, L.; Mccrate, J. M.; Leee, J.; Li, H. *Nanotechnology* **2011**, *22*, 105708.
(43) Hou, W. C.; Moghadam, B. Y.; Corredor, C.; Westerhoff, P.; Posner, J. D. *Environ. Sci. Technol.* **2012**, *46*, 1869−1876.
(44) dos Santos, T.; Varela, J.; Lynch, I.; Salvati, A.; Dawson, K. A. *PLoS One* **2011**, *6*, e24438.
(45) Thurn, K. T.; Arora, H.; Paunesku, T.; Wu, A.; Brown, E. M. B.; Doty, C.; Kremer, J.; Woloschak, G. *Nanomedicine* **2011**, *7*, 123−130.
(46) Wang, L.; Liu, Y.; Li, W.; Jiang, X.; Yinglu, J.; Wu, X.; Ligeng, X.; Qui, Y.; Zhao, K.; Wei, T.; Li, Y.; Zhao, Y.; Chen, C. *Nano Lett.* **2010**, *11*, 772−780.
(47) Dausend, J.; Musyanovych, A.; Dass, M.; Walther, P.; Schrezenmeier, H.; Landfester, K.; Mailander, V. *Macromol. Biosci.* **2008**, *12*, 1135−1143.
(48) Jiang, W.; Kim, B. Y. S.; Rutka, J. T.; Chan, W. C. W. *Nat. Nanotechnol.* **2008**, *3*, 145−150.
(49) Comfort, K. K.; Maurer, E. I.; Braydich-Stolle, L. K.; Hussain, S. M. *ACS Nano* **2011**, *5*, 10000−10008.
(50) Davina, J. H.; Lamers, G. E.; van haelst, U. J.; Kenemans, P.; Stadhouders, A. M. *Ultrastruct. Pathol.* **1994**, *6*, 275−284.